DOI: 10.1002/ejic.200500560

Charge-Transfer Phase Transition and Ferromagnetism of Iron Mixed-Valence Complexes (n-$C_nH_{2n+1})_4N[Fe^{II}Fe^{III}(dto)_3]$ (n = 3–6; dto = $C_2O_2S_2$)

Miho Itoi,*[a] Yuuki Ono,[b] Norimichi Kojima,*[b] Kenichi Kato,[c,d] Keiichi Osaka,[c,d] and Masaki Takata[c,d]

Keywords: Mixed-valence compounds / Iron / Magnetic properties / Charge transfer

The iron mixed-valence complex, (n-$C_3H_7)_4N[Fe^{II}Fe^{III}(dto)_3]$ (dto = dithiooxalato) shows a charge-transfer (CT) phase transition at T_{CT} = 122.4 K. In the vicinity of T_{CT}, the spin state changes from Fe^{II} (S = 2) – Fe^{III} (S = 1/2) (high-temperature phase: HTP) to Fe^{II} (S = 0) – Fe^{III} (S = 5/2) (low-temperature phase: LTP) accompanied by a charge transfer between Fe^{II} and Fe^{III}. This complex also undergoes a ferromagnetic transition at 7 K in the LTP. In order to investigate the mechanism of the CT phase transition and the ferromagnetism, we have systematically synthesized (n-$C_nH_{2n+1})_4N[Fe^{II}Fe^{III}(dto)_3]$ (n = 3–6), and have investigated their physical properties by magnetic susceptibility, powder X-ray diffraction measurements, and ESR spectroscopy. The compounds (n-$C_nH_{2n+1})_4N[Fe^{II}Fe^{III}(dto)_3]$ (n = 3–6) display ferromagnetic phase transitions at 7 K, 7 K (& 13 K), 19.5 K, and 22 K, respectively. For n = 3 and 4, the CT phase transitions take place at $T_{CT} \approx$ 120 K and $T_{CT} \approx$ 140 K, respectively. For n = 5 and 6, on the other hand, the CT phase transition does not occur, and the spin configuration of Fe^{II} (S = 2) and Fe^{III} (S = 1/2) corresponding to the HTP for n = 3 and 4 is stable between 2 K and 300 K. The cation size of (n-$C_nH_{2n+1})_4N^+$ (n = 3–6) acts as an effective internal pressure which induces the CT phase transition and the ferromagnetic ordering in the $[Fe^{II}Fe^{III}(dto)_3]^-_\infty$ layer. We also discuss the mechanism of the CT phase transition and the ferromagnetism induced by the charge-transfer interaction between Fe^{II} and Fe^{III}.

Introduction

Transition-metal complexes with d^4-d^7 configuration have a possibility of a spin transition between a low-spin (LS) state and a high-spin (HS) state. The spin-crossover phenomenon has gained a renewed importance through the discovery of Light Induced Excited Spin State Trapping (LIESST) for $[Fe(ptz)_6](BF_4)_2$ (ptz = 1-propyltetrazole)[1] and the thermally induced spin-crossover transition with a large thermal hysteresis around room temperature in a triazole-bridged iron(II) complex.[2,3]

One expects mixed-valence complexes with spin states situated in the spin-crossover region to display several new types of conjugated phenomena, coupled with spin and charge, between neighboring metal ions, that minimize the free energy in the whole system. To explore this possibility, we have synthesized iron mixed-valence complexes whose spin states are situated in that region. It is well-known that tris(dithiocarbamato) iron(III) complexes show the spin-crossover transition.[4] In these complexes, the Fe^{III} atom is coordinated by six S atoms. Taking account of these particulars, we have synthesized dithiooxalato-bridged iron mixed-valence complexes. (Hereafter, dithiooxalato is denoted as dto.)

Heterometal dto complexes were first synthesized by Ōkawa et al., who described the ferromagnetism of (n-$C_3H_7)_4N[M^{II}Cr^{III}(dto)_3]$ (M^{II} = Fe, Co, Ni)[5] and compared their ferromagnetic properties with those of (n-$C_4H_9)_4N[M^{II}Cr^{III}(ox)_3]$ (M^{II} = Mn, Fe, Co, Ni, Cu, ox = oxalato).[6] The structures and magnetic properties of $A[M^{II}Cr^{III}(dto)_3]$ [A^+ = Ph_4P^+, ($C_nH_{2n+1})_4N^+$, n = 3–5; M^{II} = Mn, Fe, Co] complexes were investigated by J. M. Bradly et al.,[7] who confirmed that all the complexes were ferromagnets with Curie temperatures between 5 and 16 K except for the $[Mn^{II}Cr^{III}(dto)_3]$ complex, which did not show a long-range ordering above 2 K.

Recently, we have discovered a new type of first-order phase transition at $T_{CT} \approx$ 120 K for (n-$C_3H_7)_4N[Fe^{II}Fe^{III}(dto)_3]$, where the thermally induced charge-transfer between the Fe^{II} and Fe^{III} is reversible.[8,9] This phase transition is schematically shown in Figure 1. In the high-temperature phase (HTP), the Fe^{III} (S = 1/2) and Fe^{II} (S = 2) sites are coordinated by six S atoms and six O atoms, respectively. On the other hand, in the low-temperature

[a] Institute for Solid State Physics, The University of Tokyo, Kashiwanoha 5-1-1, Kashiwa 277-8581, Chiba, Japan
Fax: +81-4-7136-3333
E-mail: itoimiho@issp.u-tokyo.ac.jp
[b] Graduate School of Arts & Sciences, The University of Tokyo, Komaba 3-8-1, Meguro-Ku, Tokyo 153-8902, Japan
Fax: +81-3-5454-6741
E-mail: cnori@mail.ecc.u-tokyo.ac.jp
[c] SPring-8/JASRI, 1-1-1 Kouto, Mikazuki-cho, Sayo-gun, Hyogo 679-5198, Japan
[d] CREST, JST 4-1-8, Honcho, Kawaguchi-shi, Saitama 332-0012 Japan

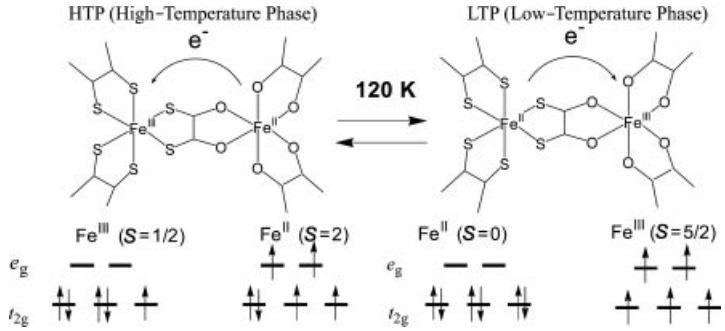

Figure 1. Schematic representation of a charge-transfer phase transition in $(n\text{-}C_3H_7)_4N[Fe^{II}Fe^{III}(dto)_3]$.

phase (LTP), the Fe^{III} (S = 5/2) site is coordinated by six O atoms, and the Fe^{II} (S = 0) site by six S atoms. Moreover, we have found a ferromagnetic transition at 7 K. The ferromagnetic interaction takes place over a long distance involving Fe^{III} (S = 5/2) – $S_2C_2O_2$ – Fe^{II} (S = 0) – $O_2C_2S_2$ – Fe^{III} (S = 5/2). The ferromagnetic ordering is presumably induced by the charge-transfer interaction between Fe^{II} and Fe^{III}.

In order to investigate the mechanism of the CT phase transition and the ferromagnetism induced by the charge-transfer interaction between Fe^{II} and Fe^{III} for $(n\text{-}C_3H_7)_4N[Fe^{II}Fe^{III}(dto)_3]$, we have synthesized iron mixed-valence complexes, $(n\text{-}C_nH_{2n+1})_4N[Fe^{II}Fe^{III}(dto)_3]$ (n = 3–6), and investigated their crystal structures and physical properties by powder X-ray diffraction, magnetic susceptibility measurements, and ESR spectroscopy. In this paper, we report our results concerning the CT phase transition and the ferromagnetic phase transition for $(n\text{-}C_nH_{2n+1})_4N[Fe^{II}Fe^{III}(dto)_3]$ (n = 3–6; the complex is hereafter denoted as n = 3–6). In addition, we discuss the mechanism of the CT phase transition and the ferromagnetism induced by the charge-transfer interaction between Fe^{II} and Fe^{III}.

Results

Structural Characterization

The crystal structure of $(n\text{-}C_3H_7)_4N[Fe^{II}Fe^{III}(dto)_3]$ has already been determined by single-crystal X-ray diffraction analysis.[10] In this compound, Fe^{II} and Fe^{III} are alternately bridged by dithiooxalato molecules, which forms the 2-D honeycomb network structure of $[Fe^{II}Fe^{III}(dto)_3]^-_\infty$. The $(n\text{-}C_3H_7)_4N^+$ cation layer is intercalated between two $[Fe^{II}Fe^{III}(dto)_3]^-_\infty$ layers. This structure is common in heterometal oxalato and dithiooxalato complexes.[11,12] The space group of $(n\text{-}C_3H_7)_4N[Fe^{II}Fe^{III}(dto)_3]$ is $P6_3$.

Single crystals of $(n\text{-}C_nH_{2n+1})_4N[Fe^{II}Fe^{III}(dto)_3]$ (n = 4–6) have not yet been obtained. However, crystals of $(n\text{-}C_nH_{2n+1})_4N[Fe^{II}Fe^{III}(dto)_3]$ (n = 4–6) appear to have honeycomb structures that are restricted to the *ab* plane. For these crystals, the lattice parameter c increases with the number of carbon atoms in $(n\text{-}C_nH_{2n+1})_4N^+$, a relationship based on results from the analogous complexes $(n\text{-}C_nH_{2n+1})_4N[M^{II}Cr^{III}(dto)_3]$ (M = Mn, Fe, Co, Ni; n = 3–5) and $A[Mn^{II}Fe^{III}(dto)_3]$ [A = $N(C_nH_{2n+1})_4$ (n = 3–5) and $P(C_6H_5)_4$].[7,13] In support of this suggestion, note that the infrared spectra of all the complexes show dto-ligand vibration bands; the ν(CO) stretching mode of the dithiooxalato molecule appears around 1500 cm^{-1}, (1490.91 cm^{-1}, 1496.0 cm^{-1}, 1490.5 cm^{-1}, and 1490.5 cm^{-1} for n = 3–6, respectively). In the case of the parent compounds $K_2(C_2O_2S_2)$ and $KBa[Fe^{III}(dto)_3]\cdot 3H_2O$, the ν(CO) vibration modes appear at higher energies (1516 cm^{-1} and 1528 cm^{-1}). The low values of ν(CO) of the n = 3–6 complexes indicate that the dto molecule acts as a bridging ligand to form the 2-D network.

The structural characteristics of $(n\text{-}C_nH_{2n+1})[Fe^{II}Fe^{III}(dto)_3]$ (n = 3–6) were investigated by powder X-ray diffraction (PXD) using synchrotron radiation. Figure 2 shows the X-ray diffraction patterns for n = 3–6 taken over 1 h at room temperature. The profiles are broad, and several peaks are only observed below $2\theta > 20°$. For the title complexes, the thermal vibration of $(n\text{-}C_nH_{2n+1})_4N^+$ appears to be quite large. A PXD measurement at low temperatures was carried out so that thermal vibration of the cation might be prevented; however, the diffraction profiles were still broad.

The sharpest peak can be attributed to the (002) reflection, which generally moves to a higher angle with decreasing temperature. The (002) reflections for $(n\text{-}C_nH_{2n+1})_4N[Fe^{II}Fe^{III}(dto)_3]$ systematically shift to lower angle as shown in Figure 2(a). These results suggest that the interlayer spacing becomes larger as the number of carbon atoms in the alkyl chains increases.

The unit cell parameters of n = 3 and 4 were estimated by the Rietveld method as shown in Figure 2(b) and (c). For the refinement of n = 4, we used the coordination of $(n\text{-}C_4H_9)_4N[Mn^{II}Fe^{III}(ox)_3]$ with the space group $P6_3$.[12] The cell parameters a are 10.06 Å (n = 3) and 10.09 Å (n = 4). The lattice parameters c are 16.18 Å (n = 3) and 18.14 Å (n = 4). The c parameter determined by PXD differs from the result of a single-crystal X-ray diffraction (SXD) study, since the h k l reflections obtained by the Rietveld analysis cover the range h = 0–3, k = 0–2, l = 0–4, a data range that is much smaller than that of the single-crystal analysis (h = 0–12, k = –12 to 10, l = –16 to 15). The error in the cell parameters in the PXD thus becomes larger than that in the SXD.

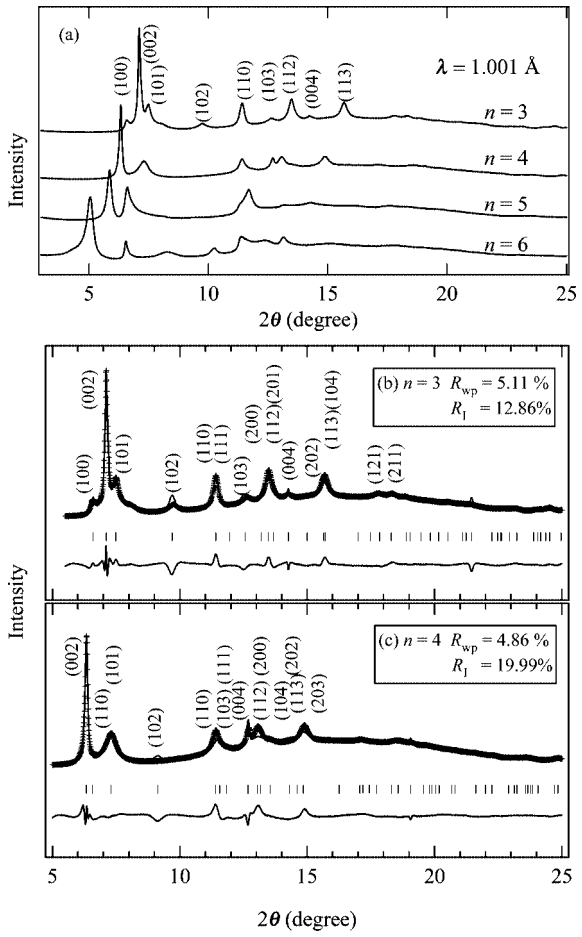

Figure 2. (a) Powder X-ray diffraction patterns for $(n\text{-}C_nH_{2n+1})_4N[Fe^{II}Fe^{III}(dto)_3]$ (n = 3–6) at room temperature. (b) Result of the Rietveld refinement for n = 3, and (c) for n = 4. R_{wp} and R_I are expressed as $\{[\Sigma_i w_i(y_i - y_{i,calc})^2/\Sigma_i w_i y_i^2]^{1/2}\}$ and $\{[\Sigma_K|I_{K,calc} - I_K|/\Sigma_K I_{K,calc}]\}$, respectively.

In the cases of n = 5 and 6, the cell parameter could not be determined by the Rietveld method. The estimated parameters of c are 19.67 Å and 22.71 Å, respectively. The lattice parameters for $(n\text{-}C_nH_{2n+1})_4N[Fe^{II}Fe^{III}(dto)_3]$ are listed in Table 1.

Table 1. Lattice parameters for $(n\text{-}C_nH_{2n+1})_4N[Fe^{II}Fe^{III}(dto)_3]$.

$(n\text{-}C_nH_{2n+1})_4N[Fe^{II}Fe^{III}(dto)_3]$	a [Å]	c [Å]	R^*, R_{WP}**
n = 3	10.06[a]	16.04[a]	0.091[a]*
	10.06[b]	16.18[b]	0.051[b]**
n = 4	10.09[b]	18.14[b]	0.049[b]**
n = 5		19.67[c]	
n = 6		22.71[c]	

[a] Value obtained from single-crystal structure analysis. [b] Refined value obtained by using the Rietveld method. [c] Calculated from the position of the (002) peak. R_{wp} is expressed as $\{[\Sigma_i w_i(y_i - y_{i,calc})^2/\Sigma_i w_i y_i^2]^{1/2}\}$.

Magnetic Properties

The static magnetic susceptibilities of n = 3–6 were measured in an external magnetic field of 5000 G. Figure 3 shows the χT and the inverse magnetic susceptibility (χ^{-1}) as a function of temperature for n = 3–6. The magnetic susceptibilities for n = 5 and 6 obey the Curie–Weiss law [$\chi^{-1} = (T - \theta)/C$] in the range 50–300 K. However, for n = 3 and 4, the magnetic susceptibilities do not obey the Curie–Weiss law over this range. The change of slope is at around 100 K on the χ^{-1} curves showing a thermal dependence. The Weiss constants are +12 K ($T_{CT} < T$: 120–300 K) and +20 K ($T_{CT} > T$: 30–98.4 K) for n = 3, +18 K ($T_{CT} < T$: 140–300 K), and +27 K ($T_{CT} > T$; 39.7–100 K) for n = 4. Those of n = 5 and 6 are +23 K and +21 K, respectively.

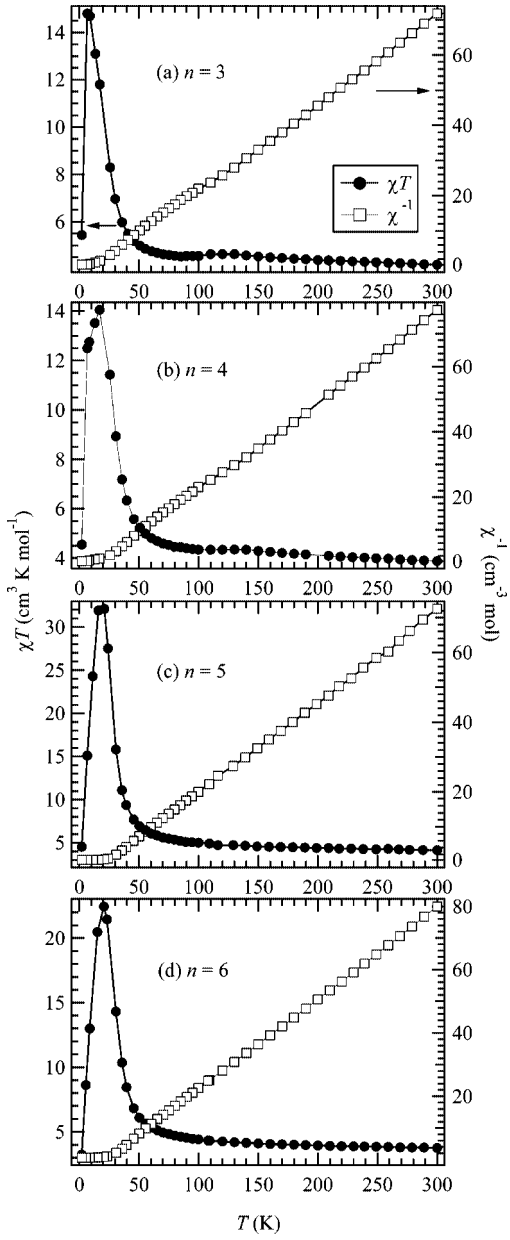

Figure 3. Temperature dependence of the magnetic susceptibility multiplied by temperature (χT) and the inverse susceptibility (χ^{-1}) of $(n\text{-}C_nH_{2n+1})_4N[Fe^{II}Fe^{III}(dto)_3]$ (n = 3–6).

All these positive Weiss constants imply the existence of a ferromagnetic interaction between Fe^{II} and Fe^{III}. At room temperature, the effective moments, μ_{eff}, are 5.87 μ_B (n = 3), 5.58 μ_B (n = 4), 5.94 μ_B (n = 5), and 5.48 μ_B (n = 6). When $kT>>|J|$, the effective moment of HTP with Fe^{II} (S = 2) and Fe^{III} (S = 1/2) is calculated as 5.91 μ_B (g = 2.00).

In order to confirm the ferromagnetic phase transition, we investigated the field-cooled magnetization (FCM), the remanent magnetization (RM) and the zero-field cooled magnetization (ZFCM) for n = 3–6, the results of which are shown in Figure 4. The FCM curve was obtained on cooling with an external magnetic field of 30 G. After the FCM measurement, the magnetic field was switched off at 2 K; then, the RM was measured from 2 K to 35 K. After cooling from 300 K to 2 K in zero external field, an external field of 30 G was switched on at 2 K. Then, the ZFCM was measured from 2 K to 35 K.

Figure 4(a) displays the FCM, RM, and ZFCM as a function of temperature for n = 3. The FCM curve shows a rapid increase below 8 K, as well as a tendency to saturate below 6 K. The RM vanishes at about 7 K. Below 7 K, the ZFCM is smaller than the FCM, a result which is due to the fact that the applied magnetic field of 30 G is too weak to move the magnetic domain walls below the ferromagnetic temperature. The ZFCM and FCM curves overlap at 7 K, where the magnetic hysteresis disappears. From these results, we estimate the Curie temperature to be 7 K. The FCM and ZFCM curves for n = 4, provided in Figure 4(b), are different from those for n = 3. The FCM has a shoulder at 13 K and the ZFCM has two peaks at 7 K and 13 K. The RM vanishes at 13 K, where the ZFCM and FCM meet each other. The ZFCM of n = 4 implies that two ferromagnetic phases with Tc = 7 K and 13 K coexist, which we can regard as a mixture of HTP and LTP at a low temperature. The coexistence of HTP and LTP is consistent with the ESR data. Figure 4(c) and (d) show the temperature dependences of the magnetizations for n = 5 and 6. The FCM steeply increases at 23 K and 26 K for n = 5 and 6, respectively, and the RM disappears at 19 K and 25 K for n = 5 and n = 6, respectively, where the ZFCM and FCM curves meet each other. The Curie temperatures for n = 3–6 were evaluated at 7 K, 7 K (&13 K), 19.5 K and 22 K, respectively, from heat capacity measurements (for n = 3 and 4),[14,15] and by an *Arrott plot*,[16] i.e. $M^2 - H/M$ ($1/\chi$) plot (for n = 5 and 6). The Curie temperatures for n = 3–6 are listed in Table 2.

Reflecting the CT phase transition, a small bump appears in the χT curve and the slope of χ^{-1} changes around 120 K (n = 3) and 140 K (n = 4). We carefully measured the magnetic susceptibility for n = 3 and 4 with a sweep rate of 0.1 K min^{-1} on heating and cooling, the results of which are shown in Figure 5. A thermal hysteresis loop appears between 60 K and 130 K for n = 3, and between 50 K and 150 K for n = 4. The χT curve for n = 4 changes by about 4% between 50 K and 150 K. This value is smaller than that for n = 3, which drops by about 7% between 60 K and 130 K.

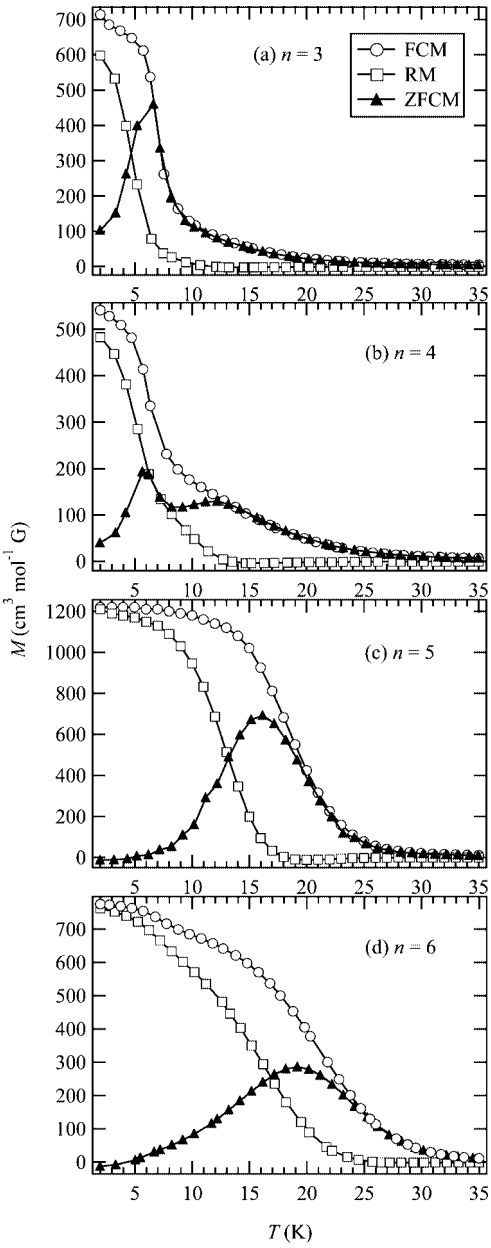

Figure 4. Temperature dependence of the field cooled magnetization (FCM:○), the remnant magnetization (RM:□), and the zero-field cooled magnetization (ZFCM:▲) for $(n\text{-}C_nH_{2n+1})_4N[Fe^{II}Fe^{III}(dto)_3]$ (n = 3–6). Applied magnetic field H = 30 G.

ESR Spectroscopy

In order to investigate the CT phase transition and the spin state of the Fe atom, we obtained the ESR spectra for n = 3–6 between 4 K and 300 K. The experimental conditions are as described in ref.[17]

Figure 6 shows the temperature dependence of the ESR signal of the n = 3 complex. When the temperature was lowered from room temperature, an ESR signal corresponding to the Fe^{III} site with S = 5/2 appeared below 105 K, and its intensity strengthened with decreasing temperature. On heating, the ESR signal vanished above 130 K. The g value of the ESR signal at the center of the 3200-G

Table 2. The parameters related to the change-transfer phase transition and ferromagnetism for $(n\text{-}C_nH_{2n+1})_4N[Fe^{II}Fe^{III}(dto)_3]$ (n = 3–6).

	$(n\text{-}C_nH_{2n+1})_4N[Fe^{II}Fe^{III}(dto)_3]$ (n = 3-6)			
	n = 3	n = 4	n = 5	n = 6
Charge-Transfer Phase Transition	$T_{CT\downarrow}$* = 60 K	$T_{CT\downarrow}$ = 50 K	-	-
	$T_{CT\uparrow}$* = 130 K	$T_{CT\uparrow}$ = 145 K	-	-
Spin State of Fe				
Fe^{II}	$S = 2$ ($T > T_{CT}$)	$S = 2$ ($T > T_{CT}$)	$S = 2$	$S = 2$
	$S = 0$ ($T < T_{CT}$)	$S = 0$ ($T < T_{CT}$)		
Fe^{III}	$S = 1/2$ ($T > T_{CT}$)	$S = 1/2$ ($T > T_{CT}$)	$S = 1/2$	$S = 1/2$
	$S = 5/2$ ($T < T_{CT}$)	$S = 5/2$ ($T < T_{CT}$)		
Curie Constant (cm^3 K mol^{-1})	3.90**	3.56**	3.88	3.52
T_C (K)***	7	7 (13 K)	19,5	22
Weiss Constant (K)	+12 (HTP), +20 (LTP)	+18 (HTP), +27 (LTP)	+23	+21
Coercive Field at 2 K (G)	310	3160	6600	6800

* $T_{CT\uparrow}$ and $T_{CT\downarrow}$ denote, respectively, the upper-limit and the lower-limit of the thermal hysteresis loop for the charge-transfer phase transtion.
** Curie constants were estimated in the high-temperature phase (HTP).
*** Curie temperatures of $(n\text{-}C_nH_{2n+1})_4N[Fe^{II}Fe^{III}(dto)_3]$ were determined by heat capacity measurements (for n = 3, 4) and by Arrott plots (for n = 5, 6).

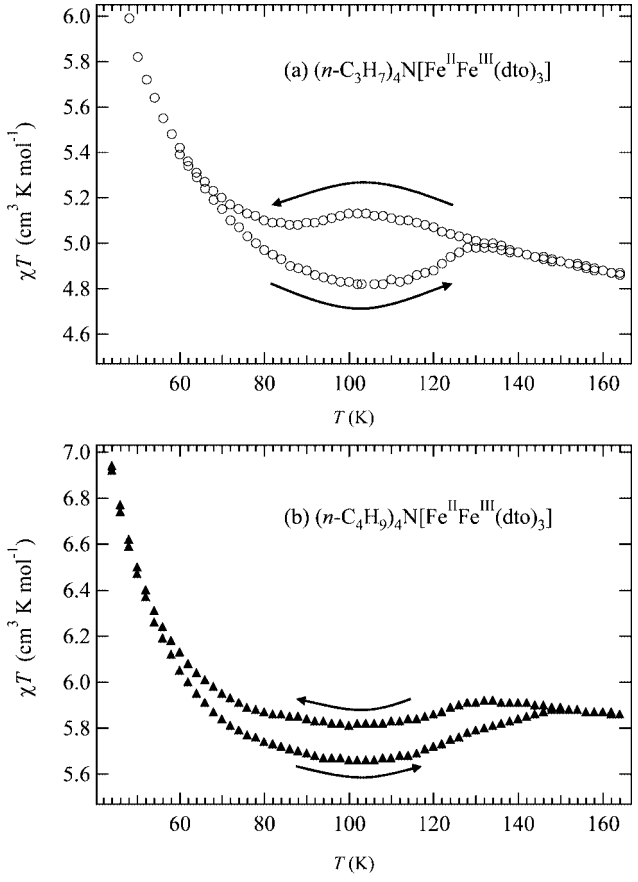

Figure 5. Temperature dependence of the magnetic susceptibility for $(n\text{-}C_3H_7)_4N[Fe^{II}Fe^{III}(dto)_3]$ and $(n\text{-}C_4H_9)_4N[Fe^{II}Fe^{III}(dto)_3]$. Temperature sweep rate is 0.1 K min^{-1}; (→) and (←) denote heating and cooling, respectively.

field is 2.10, which is consistent with that of the HS state ($^6A_{1g}$) of Fe^{III}, whose spin-orbit interaction is negligibly small. The half width (ΔH_{pp}) has an almost constant value of ΔH_{pp} = 1470 G between 60 K and 120 K. In the case of n = 4, as shown in Figure 7, a similar ESR signal corresponding to the HS state ($^6A_{1g}$) of Fe^{III} appeared below 105 K in the cooling mode. On heating, the ESR signal almost disappeared above 145 K. The ΔH_{pp} for n = 4 has an almost constant value of 1600 G between 50 and 140 K. In addition to the ESR signal due to the HS state ($^6A_{1g}$) of Fe^{III}, a weak signal is observed at 1600 G, whose g value is 4.1. This weak signal should be attributed to the HTP fraction, i.e. the HS state (S = 2; $^5T_{2g}$) of the Fe^{II} and/or the LS state (S = 1/2; $^2T_{2g}$) of the Fe^{III}. For n = 5 and 6, a similar ESR signal appears at about 1600 G. Therefore, the HTP coexists with the LTP at 20 K for n = 4, a finding which could account for the existence of the two peaks in the ZFCM.

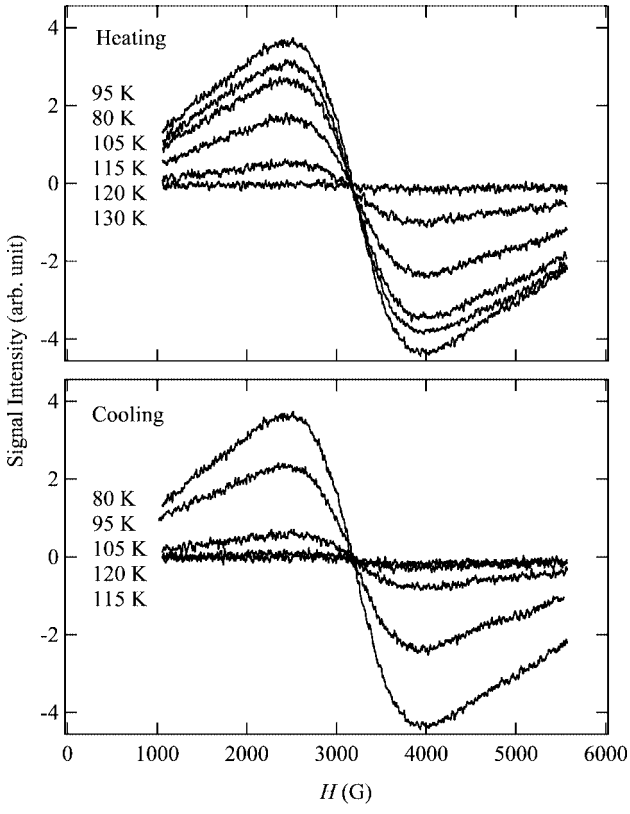

Figure 6. Temperature dependence of the ESR spectra on heating and cooling for $(n\text{-}C_3H_7)_4N[Fe^{II}Fe^{III}(dto)_3]$.

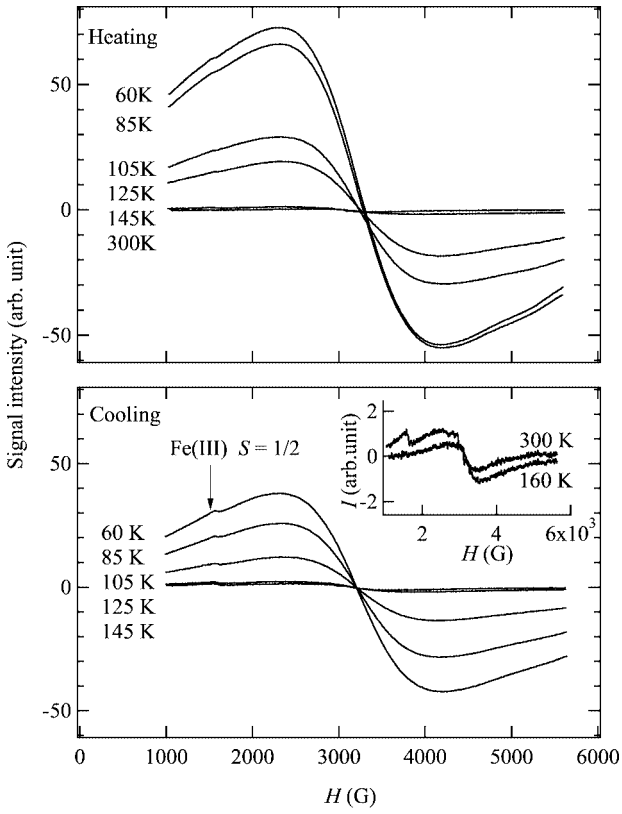

Figure 7. Temperature dependence of the ESR spectra on heating and cooling for $(n\text{-}C_4H_9)_4N[Fe^{II}Fe^{III}(dto)_3]$. Inset denotes the ESR signal corresponding to the Fe^{III} ($^2T_{2g}$, S = 1/2) of the HTP at 160 K and room temperature.

We estimated the spin susceptibilities corresponding to the HS state ($^6A_{1g}$) of the Fe^{III} atom for n = 3 and 4. The spin susceptibility is expressed as $\chi_{spin} = A(I(H) \times \{\Delta H_{PP}\}^2)$, where A is a constant value, $I(H)$ is the signal intensity, and ΔH_{PP} is the half width.[18] The spin susceptibilities for n = 3 and n = 4 are shown in Figure 8. The large thermal hysteresis loop in χ_{spin} for n = 4 is in good agreement with that of the dc magnetic susceptibility; however, the thermal hysteresis loop in χ_{spin} for n = 3 is narrower than that of the dc magnetic susceptibility.

In the cases of $KBa[Fe^{III}(dto)_3]\cdot 3H_2O$ and $(n\text{-}C_nH_{2n+1})_4N[Fe^{II}Fe^{III}(dto)_3]$ (n = 5 and 6), the ESR spectra are completely different from those of n = 3 and 4. For n = 5 and 6, we could not observe a drastic signal change caused by the CT phase transition such as we noted for n = 3 and 4. The ESR signals of n = 5 and 6 are shown in Figure 9. The ESR spectra of the parent complex, $KBa[Fe^{III}(dto)_3]\cdot 3H_2O$, is shown in Figure 9(a). The paramagnetic spin of $KBa[Fe^{III}(dto)_3]\cdot 3H_2O$ has been already reported as the Fe^{III} LS state (S = 1/2) on the basis of magnetic susceptibility and Mössbauer spectroscopy results.[11,19,20]

The $KBa[Fe^{III}(dto)_3]\cdot 3H_2O$ complex has two ESR signals: a strong signal at 1600 G, and a weak signal at 3200 G. The g values of the ESR signals at 1600 G and 3200 G are estimated at 4.10 and 2.01 and are attributed to the $g_\perp$ and $g_\parallel$ of Fe^{III} (S = 1/2), respectively. However, the ESR signal with g = 2.01 persisted at room temperature, even though

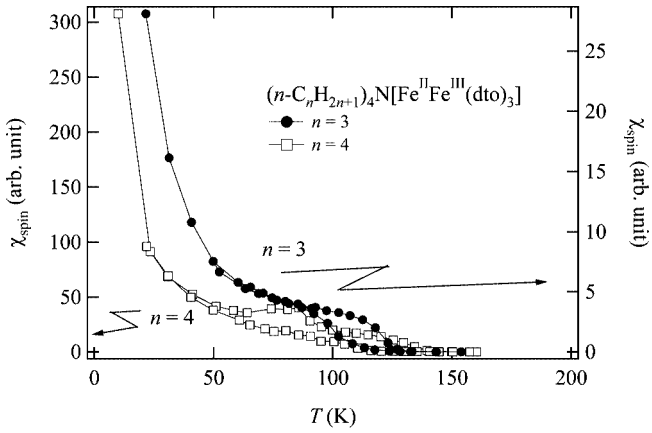

Figure 8. Temperature dependence of the spin susceptibility for $(n\text{-}C_nH_{2n+1})N[Fe^{II}Fe^{III}(dto)_3]$ (n = 3 and 4).

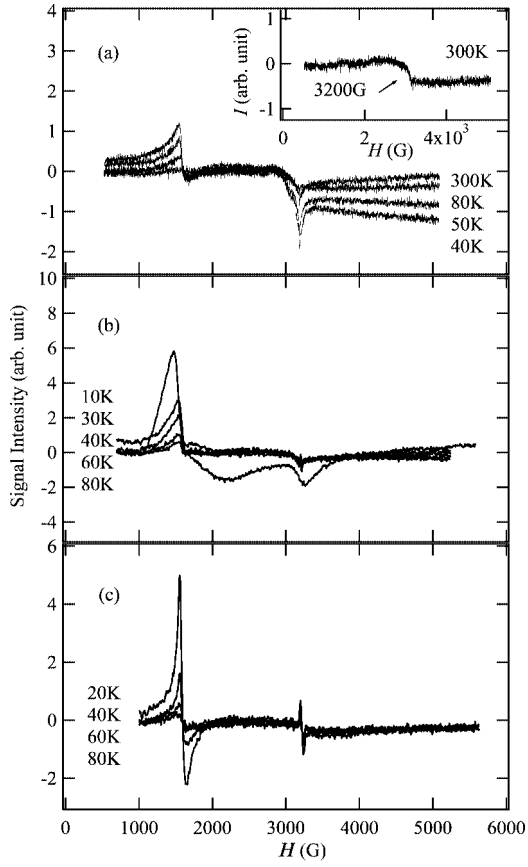

Figure 9. The ESR spectra at several temperatures for (a) $KBa[Fe^{III}(dto)_3]\cdot 3H_2O$; (b) $(n\text{-}C_5H_{11})_4N[Fe^{II}Fe^{III}(dto)_3]$; and (c) $(n\text{-}C_6H_{13})_4N[Fe^{II}Fe^{III}(dto)_3]$.

the strong signal with g = 4.10 disappeared above 90 K. Therefore, we suggest that the HS state (S = 5/2) of the Fe^{III} atom caused by linkage isomerization ($Fe^{III}O_4S_2$ and / or $Fe^{III}O_6$) is responsible for this appearance of the ESR signal around 3200 G at room temperature. The ^{57}Fe Mössbauer spectrum for $KBa[Fe^{III}(dto)_3]\cdot 3H_2O$ did not enable us to distinguish the minor fraction of the Fe^{III} HS state (S = 5/2) caused by linkage isomerization from the LS state (S = 1/2), because these Mössbauer spectra appear at almost

the same velocities. Therefore, the ESR signal due to the Fe^{III} HS state (S = 5/2) is presumably superposed on the ESR signal with $g_{\parallel}$ = 2.01 corresponding to the Fe^{III} LS state (S = 1/2).

For n = 5 and 6, the ESR spectra were quite similar to those of $KBa[Fe^{III}(dto)_3]\cdot 3H_2O$. A strong signal at 1580 G and a weak signal at 3260 G were observed. The g values of the ESR signals at 1580 G and 3260 G are estimated at 4.10 and 2.01, respectively, which are attributed to the $g_{\perp}$ and $g_{\parallel}$ of the LS state (S = 1/2) of Fe^{III}. The signal with g = 2.01 persisted at room temperature, so that an ESR signal due to the HS state (S = 5/2) of the Fe^{III} atom caused by linkage isomerization ($Fe^{III}O_4S_2$ and /or $Fe^{III}O_6$) appeared around 3260 G. Note that the ratio of the linkage isomer $Fe^{II}O_4S_2$ (S = 2) can be estimated easily by Mössbauer spectroscopy. The percentages of the linkage isomer of $Fe^{II}O_4S_2$ are about 8% at 60 K for n = 3, 14% at 25 K for n = 4, 4% at 25 K for n = 5, and 11% at 30 K for n = 6. The $Fe^{II}O_4S_2$ persists at low temperatures without creating charge-transfer.[21]

In the cases of n = 5 and 6, the ESR signals of the LS state (S = 1/2) of the Fe^{III} atom decrease with increasing temperature and then almost disappear above 90 K; the latter change takes place because of rapid spin-lattice relaxation. The ESR signal of the HS state ($^5T_{2g}$) of Fe^{II} and the LS state ($^2T_{2g}$) of Fe^{III} could not be observed in the high-temperature region. From the analysis of the ESR spectra, we conclude that the CT phase transition does not take place for n = 5 and 6, in which the spin configurations of Fe^{II} (S = 2) and Fe^{III} (S = 1/2) are stable between 4 K and 300 K.

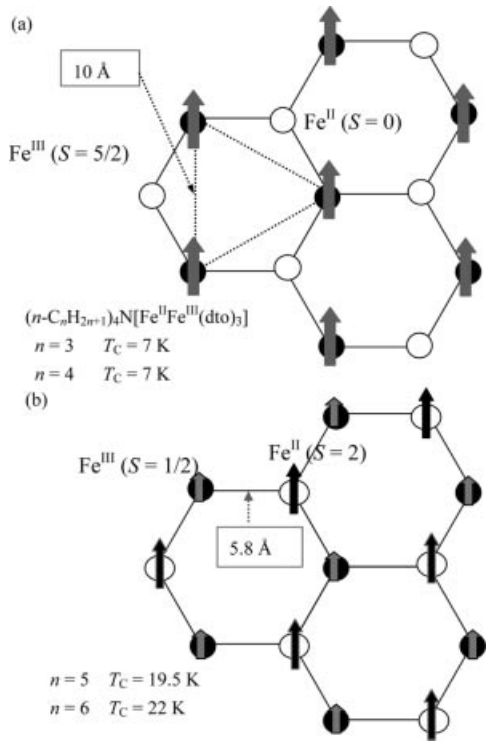

Figure 10. Schematic representation of ferromagnetic ordering for $(n\text{-}C_nH_{2n+1})_4N[Fe^{II}Fe^{III}(dto)_3]$ (n = 3–6). (a) The ferromagnetic ordering for n = 3 and n = 4 takes place in the LTP with the spin configuration Fe^{II} (S = 0) and Fe^{III} (S = 5/2). (b) The ferromagnetic ordering for n = 5 and n = 6 takes place in the HTP with the spin configuration Fe^{II} (S = 2) and Fe^{III} (S = 1/2).

Discussion

The spin state in the paramagnetic-ferromagnetic region and the existence of the charge-transfer phase transition of $(n\text{-}C_nH_{2n+1})_4N[Fe^{II}Fe^{III}(dto)_3]$ (n = 3–6) are revealed by magnetic susceptibility measurements and ESR spectroscopy. The appearance of the CT phase transition and the mechanism of the ferromagnetism in an iron mixed-valence tris-dithiooxalato complex critically depend on the cation size $(n\text{-}C_nH_{2n+1})_4N^+$ (n = 3–6). The CT phase transitions are observed for n = 3 (120 K) and 4 (140 K), and then the Fe^{II} (S = 0) – Fe^{III} (S = 5/2) spin combination causes the ferromagnetic transition at 7 K. On the other hand, the CT phase transition is not apparent for n = 5 and n = 6; Fe^{II} (S = 2) – Fe^{III} (S = 1/2) spins are stable between 2 K and 300 K. The spin configuration corresponding to the HTP of n = 3 and 4 is responsible for the ferromagnetic transitions at 19.5 K (n = 5) and 22 K (n = 6), respectively. The ferromagnetically ordered states and several parameters for n = 3–6 are schematically shown in Figure 10 and Table 2.

Due to the effect of the cation size, the $[Fe^{II}Fe^{III}(dto)_3]$ layers are separated by an increment corresponding to the length of the alkyl chain from n = 3 to n = 6. The bulkier $(n\text{-}C_nH_{2n+1})_4N^+$ cations probably expand or distort slightly the $[Fe^{II}Fe^{III}(dto)_3]$ honeycomb ring. The cell parameter a of the analogous complexes, $(n\text{-}C_nH_{2n+1})_4N[Fe^{II}Fe^{III}(ox)_3]$ (n = 3–5)[22] tends to expand slightly as n increases. For n = 4, the slight expansion or distortion of the 2-D honeycomb ring (Δa = 0.03 Å) might be expected to lead to an inhibition of CT between the Fe atoms; thus, the HTP spin partially remains at low temperature. We should note that n = 5 shows a CT phase transition under 0.5 GPa, and the ferromagnetic transition temperature changes from 19.5 K to 7 K. In other words, the spin configuration changes from Fe^{II} (S = 2) – Fe^{III} (S = 1/2) (HTP) to Fe^{II} (S = 0) – Fe^{III} (S = 5/2) (LTP).[23] There is a limiting size of the honeycomb ring between n = 4 and n = 5 where the CT does not occur. Unfortunately, we could not obtain information on the crystal structure of the $(n\text{-}C_nH_{2n+1})_4N[Fe^{II}Fe^{III}(dto)_3]$ (n = 5, 6) complexes by PXD. A single crystal X-ray analysis of the n = 4–6 and an X-ray diffraction measurement taken under pressure are necessary to quantitatively clarify the cation size effects on the $[Fe^{II}Fe^{III}(dto)_3]^-$ layer.

The mechanism of the magnetic interaction in the iron tris-dithiooxalato complexes is dramatically changed according to whether a CT phase transition exists. Here, we will discuss the origin of the magnetic interaction in the title complexes. The ferromagnetic ordering for n = 3 and 4 is considered to be established by the charge-transfer interaction between Fe^{II} and Fe^{III}, the same mechanism as in $Fe^{III}_4[Fe^{II}(CN)_6]_3\cdot 15H_2O$ (T_C = 5.5 K),[24,25] as shown in Fig-

ure 11(a). In contrast, for n = 5 and 6, the spin configuration of Fe^{II} (S = 2) and Fe^{III} (S = 1/2) is the ground state between 2 K and 300 K. The ferromagnetic ordering for n = 5 and 6 is schematically shown in Figure 11(b); each Fe^{III} site in the LS state (S = 1/2) accepts a t_2 electron with a down-spin from the neighboring Fe^{II} site in the HS state (S = 2). Therefore, the coupling between the ground configuration $\varphi_i[Fe^{III}(t_2^5)]\varphi_j[Fe^{II}(t_2^4e^2)]$ and the charge-transfer configuration $\varphi_i[Fe^{II}(t_2^6)]\varphi_j[Fe^{III}(t_2^3e^2)]$ stabilizes the ground state, a situation favoring ferromagnetic ordering. In the ground configuration of $\varphi_i[Fe^{III}(t_2^5)]\varphi_j[Fe^{II}(t_2^4e^2)]$, in addition to the charge-transfer interaction, the potential exchange interaction due to the orbital orthogonality between the t_2 electron with an up-spin Fe^{III} and the Fe^{II} electrons with up-spins (in e orbitals and one t_2 orbital) induces ferromagnetic ordering, which is presumably responsible for the ferromagnetic transition with a high T_C in n = 5 and 6.

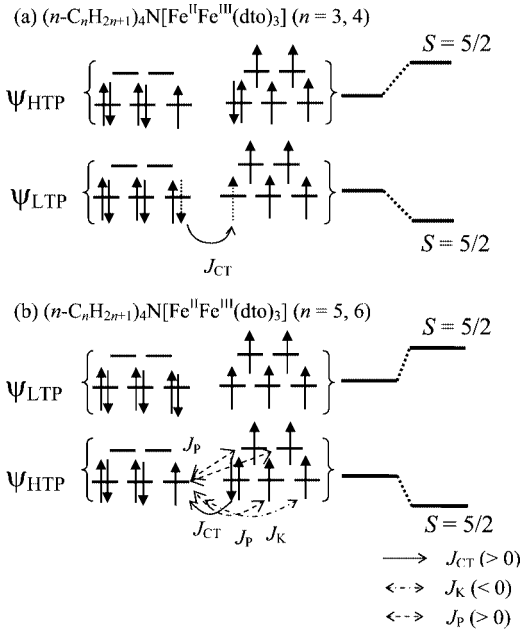

Figure 11. (a) Ferromagnetism induced by the charge-transfer interaction between Fe^{II} (S = 0) and Fe^{III} (S = 5/2) for (n-C_nH_{2n+1})$_4$N[$Fe^{II}Fe^{III}$(dto)$_3$] (n = 3, 4). (b) Ferromagnetism induced by the charge-transfer interaction as well as the potential exchange interaction between Fe^{II} (S = 2) and Fe^{III} (S = 1/2) for (n-C_nH_{2n+1})$_4$N[$Fe^{II}Fe^{III}$(dto)$_3$] (n = 5, 6). Solid line arrow: charge transfer interaction ($J_{CT} > 0$); dash-dotted line arrow: kinetic exchange interaction ($J_K < 0$); short-dashed line arrow: potential exchange interaction ($J_P > 0$).

Next, to quantify the ferromagnetic interaction between the iron atoms of (n-C_nH_{2n+1})$_4$N[$Fe^{II}Fe^{III}$(dto)$_3$] (n = 3–6), we will estimate the exchange interaction J in a 2-D layer by means of the simplest Hamiltonian,

$$H = -J\sum_{<i,j>}\vec{S}_i\cdot\vec{S}_j - gh\sum_i S_i^Z .$$

Here, h is the external magnetic field. For n = 3 and 4, the LTP spin state with Fe^{III}(S = 5/2) – Fe^{II}(S = 0) appears via a CT phase transition, and the states produce large triangular interactions in the 2-D plane [Figure 10(a)]. In the case of the triangular lattice, the number of nearest neighbors of the Fe^{III} (S = 5/2) site is 6. The molar susceptibility of the triangular lattice, calculated by a high-temperature expansion up to the second order, is given by [Equation (1)]:[26]

$$\chi = \frac{NS(S+1)}{3}\beta(g\mu_B)^2 + \frac{2N\beta^2\mu_B^2g^2}{3}JS^2(S+1)^2 \qquad (1)$$

Here β is $1/kT$, N is Avogadro's number, and μ_B is the Bohr magneton. After substituting S = 5/2 and g = 2.00 into (1), we estimate the exchange coupling by the least-squares method. The fitting curves are shown in Figure 12(a). The range analyzed in the LTP is from 20 to 122 K for n = 3, and from 20 to 140 K for n = 4. The values obtained are J = 3.12 K for n = 3, and 2.39 K for n = 4.

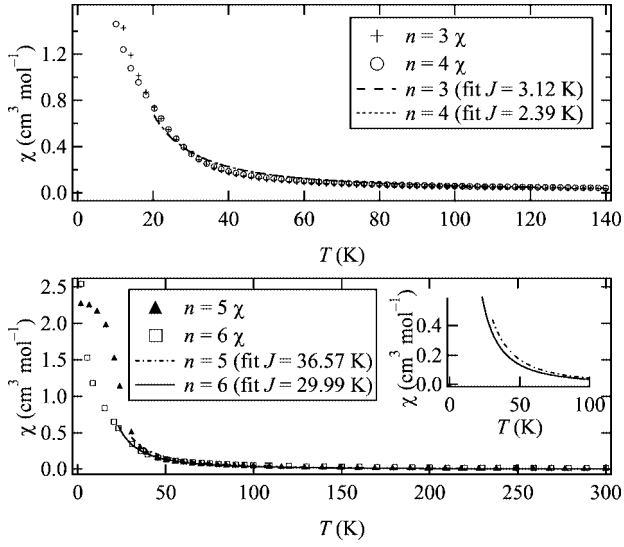

Figure 12. Temperature dependences of χ for n = 3–6 with high-temperature expansion fitting. (a) dashed line: fitting for n = 3; short-dashed line: fitting for n = 4 in LTP spin configuration (Fe^{III} S = 5/2 – Fe^{II} S = 0) on triangular lattice. Molar susceptibility for n = 3 and 4 is indicated by plus (+) and circle (○) symbols, respectively. (b) dash-dotted line: fitting for n = 5; solid line: fitting for n = 6 in HTP spin configuration (Fe^{III} S = 1/2 – Fe^{II} S = 2) on hexagonal lattice. Molar susceptibility for n = 5 and 6 is indicated by the solid triangle (▲) and square (□) symbols, respectively.

On the other hand, for n = 5 and 6, there is no CT phase transition, and the Fe^{III} (S = 1/2) – Fe^{II} (S = 2) interaction takes place on hexagonal rings [Figure 10(b)]. In the case of a hexagonal lattice, the number of nearest neighbors is 3. For n = 5 and 6, the Fe^{II} (S = 2) atom is connected with three Fe^{III} (S = 1/2) atoms. The high-temperature expansion of the susceptibility for a hexagonal lattice is calculated by the same procedure as (1), and we get the molar susceptibility as follows [Equation (2)]:

$$\chi = \frac{N\beta\mu_B^2}{6}(g_AS_A(S_A+1)+g_BS_B(S_B+1)) + \frac{N\beta^2\mu_B^2}{3}g_Ag_BJS_A(S_A+1)S_B(S_B+1) \qquad (2)$$

After substituting S_A = 1/2 and S_B = 2 into (2), we estimated the exchange coupling and g values by the least-squares method. The range analyzed is from 31 to 300 K for n = 5, and from 21 to 300 K for n = 6. Then, we obtained J = 36.57 K for n = 5 and J = 29.99 K for n = 6, with $g_{1/2}$ = g_2 = 4.00 values, which were in agreement with the T_C and g values obtained by the ESR spectra. The fitting curves are shown in Figure 12(b). The ferromagnetic interactions J for n = 3 and 4 are considerably lower than those for n = 5 and 6.

Conclusion

We have synthesized (n-C_nH_{2n+1})$_4$N[$Fe^{II}Fe^{III}$(dto)$_3$] (n = 3–6), and have investigated the cation-size effect on the CT phase transition and the ferromagnetic transition in these compounds. The result of our PXD measurement confirmed that the 2-D honeycomb network layer [$Fe^{II}Fe^{III}$(dto)$_3$]$^-$ is increasingly well separated with increases in the number n of the (n-C_nH_{2n+1})$_4$N cations. We have also determined, by magnetic susceptibility and ESR spectroscopy measurements, the spin states of the Fe^{II} and Fe^{III} sites for n = 3–6 between 2 and 300 K. The (n-C_nH_{2n+1})$_4$N$^+$ cation size affects the existence or nonexistence of the CT phase transition and the ferromagnetic interaction J between the Fe^{II} and Fe^{III} sites. For n = 3 and 4, we observed the thermally induced charge transfer between Fe^{II} and Fe^{III} around 120 K (n = 3) and 140 K (n = 4). The spin configuration changes from Fe^{II} (S = 2) – Fe^{III} (S = 1/2) (HTP) to Fe^{II} (S = 0) – Fe^{III} (S = 5/2) (LTP) in the vicinity of the CT phase transition temperature (T_{CT}). Furthermore, the Fe^{III} (S = 5/2) spin, which is located on a large triangular lattice, is ferromagnetically ordered at 7 K. On the other hand, for n = 5 and 6, the CT phase transition did not occur, and the spin configuration of the HTP for n = 3 and 4 dominated over the whole temperature range. The Fe^{II} (S = 2) – Fe^{III} (S = 1/2) spin configurations located on a hexagonal lattice produce the ferromagnetic transitions at 19.5 K (n = 5) and 22 K (n = 6), respectively.

Experimental Section

Syntheses

$K_2C_2O_2S_2$: Potassium dithiooxalate, $K_2C_2O_2S_2$, was prepared by the reaction of potassium hydrogensulfide KHS (14.57 g, 0.20 mol) and di-*n*-pentyl dithiooxalate (n-C_5H_{11})$_2$($C_2O_2S_2$) (0.10 mol) in methanol. The di-*n*-pentyl dithiooxalate was obtained by the reaction of oxalyl dichloride $(COCl)_2$ (8.61 mL, 0.10 mol) and 1-pentanethiol $CH_3(CH_2)_4SH$ (25 mL, 0.20 mol). After filtration, the $K_2C_2O_2S_2$ was washed well with methanol to remove the KHS and, because $K_2C_2O_2S_2$ is highly hygroscopic,[27,28] it was dried in vacuo. $C_2K_2O_2S_2$ (198.35): calcd. C 12.11, S 32.33; found C 12.28, S 32.54.

KBa[Fe^{III}(dto)$_3$]·3H_2O: $Fe(NO_3)_3$·10H_2O (2.10 g, 5.61·10^{-3} mol) was treated with $K_2C_2O_2S_2$ (3.00 g, 15.1 mmol) in cold water (25 mL), and the solution was filtered to remove iron sulfide. Then $BaBr_2$·2H_2O (2.50 g, 0.17 mol) was added to the dark purple solution, and KBa[Fe^{III}(dto)$_3$]·3H_2O precipitated. The salt was recrystallized from water and dried for one day.[20,29,30] $C_6H_6BaFeKO_9S_6$ (646.8): calcd. C 11.14, H 0.94, S 29.75; found C 11.39, H 1.20, S 29.66.

(n-C_nH_{2n+1})$_4$N[$Fe^{II}Fe^{III}$(dto)$_3$] (n = 3–6): The title complexes were synthesized in a way similar to the preparation of (n-C_3H_7)$_4$N-[$M^{II}Cr^{III}$(dto)$_3$] (M = Fe, Co, Ni, Zn).[5]

A solution of KBa[Fe(dto)$_3$]·3H_2O (0.5 g, 0.77 mmol) in a 3:2 methanol/water mixture (20 mL) was stirred. To this was added slowly a solution of $FeCl_2$·4H_2O (0.24 g, 0.77 mmol) and (n-C_nH_{2n+1})$_4$NBr (n = 3–6) (1.15 mmol) in a 3:2 methanol/water mixture (20 ml), whereupon a black powdered crystal precipitated. The compounds (n-C_nH_{2n+1})$_4$N[$Fe^{II}Fe^{III}$(dto)$_3$] (n = 3–6) were separated as powdered crystals by suction filtration and washed first with a 1:1 methanol/water mixture and then with methanol and diethyl ether. The compounds (n-C_nH_{2n+1})$_4$N[$Fe^{II}Fe^{III}$(dto)$_3$] (n = 7, 8) could not be obtained as crystalline powders. The elemental analysis for the precipitated crystal that had been stirred at 30–40 °C for 12 h was in good agreement with the calculated one; the results are listed in Table 3.

Table 3. Elemental analysis of C, H, N, and S in (n-C_nH_{2n+1})$_4$N-[$Fe^{II}Fe^{III}$(dto)$_3$] (n = 3–6).

(n-C_nH_{2n+1})$_4$N[$Fe^{II}Fe^{III}$(dto)$_3$]	C	H	N	S
n = 3 found (calc)	32.88 (32.83)	4.46 (4.29)	2.34 (2.13)	29.40 (29.22)
n = 4	36.73 (36.98)	5.14 (5.08)	1.76 (1.96)	27.33 (26.92)
n = 5	40.71 (40.52)	5.93 (5.75)	1.64 (1.82)	24.72 (24.96)
n = 6	43.78 (43.58)	6.58 (6.34)	1.64 (1.69)	23.23 (23.27)

Measurements: The powder X-ray diffraction data was taken at the BL02B2 beam line of SPring-8.[31] The as-grown powdered sample was sealed in a Lindemann capillary having a diameter of 0.3 mm, which gave a homogeneous intensity distribution in the Debye–Scherrer ring. The wavelength of the X-ray was 1.001 Å, and the exposure time at 300 K was 1 h. The static magnetic susceptibility was measured with a Quantum Design MPMS5 SQUIID magnetometer. Powdered crystals (10 mg) were wrapped in a polyethylene film and held in a plastic straw. The magnetic susceptibility obtained was corrected for the background and the core diamagnetism. The diamagnetic correction for constituting atoms was carried out using Pascal's constants.[32] The diamagnetic Pascal's corrections are as follows: –4.18·10^{-4} cm^3 mol^{-1} (n = 3), –4.66·10^{-4} cm^3 mol^{-1} (n = 4), –5.13·10^{-4} cm^3 mol^{-1} (n = 5), and –5.60·10^{-4} cm^3 mol^{-1} (n = 6). The ESR spectra for the powdered crystals were obtained with a JEOL JES-TE300 X-band ESR spectrometer. The magnetic field was monitored with an Echo Electronics ES-FC5 field meter.

Acknowledgments

The authors wish to thank Prof. K. Asai, Prof. Y. Uwatoko, Prof. F. Varret, Prof. K. Boukheddaden, Prof. C. Itoi, Dr. Y. Kobayashi, and Dr. M. Enomoto for many helpful discussions. This work was supported by a Grant-in-Aid for Scientific Research and a Grant-in-Aid from the 21st Century COE (Center of Excellence) Program (Research Center for Integrated Science) of the Japanese Ministry of Education, Science, Sports, and Culture. The synchrotron-radiation X-ray powder experiments were performed at the SPring-8 BL02B2 with approval of the Japanese Synchrotron Radiation Research Institute (JASRI). One of the authors (M. Itoi) was sup-

ported by Research Fellowships of the Japanese Society for the Promotion of Science for Young Scientists.

[1] S. Decurtins, P. Gütlich, C. P. Köhler, H. Spiering, A. Hauser, *Chem. Phys. Lett.* **1984**, *105*, 1–4.
[2] J. Kröber, E. Codjovi, O. Kahn, F. Grolière, C. Jay, *J. Am. Chem. Soc.* **1993**, *115*, 9810–9811.
[3] O. Kahn, C. J. Martinez, *Science* **1998**, *279*, 44.
[4] L. Cambi, A. Cagnasso, *Atti Accad. Naz. Lincei* **1931**, *13*, 809–813.
[5] H. Ōkawa, M. Mitsumi, M. Ohba, M. Kodera, N. Matsumoto, *Bull. Chem. Soc. Jpn.* **1994**, *67*, 2139–2144.
[6] H. Tamaki, Z. J. Zhong, N. Matsumoto, S. Kida, M. Koikawa, N. Achiwa, Y. Hashimoto, H. Ōkawa, *J. Am. Chem. Soc.* **1992**, *114*, 6974–6979.
[7] J. M. Bradly, S. G. Carling, D. Visser, P. Day, D. Hautot, G. J. Long, *Inorg. Chem.* **2003**, *42*, 986–996.
[8] N. Kojima, W. Aoki, M. Seto, Y. Kobayashi, Yu. Maeda, *Synth. Met.* **2001**, *121*, 1796–1797.
[9] N. Kojima, W. Aoki, M. Itoi, Y. Ono, M. Seto, Y. Kobayashi, Yu. Maeda, *Solid State Commun.* **2001**, *120*, 165–170.
[10] M. Itoi, A. Taira, M. Enomoto, N. Matsushita, N. Kojima, Y. Kobayashi, K. Asai, K. Koyama, T. Nakano, Y. Uwatoko, *Solid State Commun.* **2004**, *130*, 415–420.
[11] Y. Ono, M. Okubo, N. Kojima, *Solid State Commun.* **2003**, *126*, 291–296.
[12] R. Pellaux, H. W. Schmalle, R. Huber, P. Fischer, T. Hauss, B. Ouladdiaf, S. Decurtins, *Inorg. Chem.* **1997**, *36*, 2301–2308.
[13] S. G. Carling, J. M. Bradley, D. Visser, P. Day, *Polyhedron* **2003**, *22*, 2317–2324.
[14] T. Nakamoto, Y. Miyazaki, M. Itoi, Y. Ono, N. Kojima, M. Sorai, *Angew. Chem. Int. Ed.* **2001**, *40*, 4716–4719.
[15] T. Nakamoto, Y. Miyazaki, M. Itoi, Y. Ono, N. Kojima, M. Sorai, to be submitted.
[16] A. Arrott, *Phys. Rev.* **1957**, *108*, 1394–1396.
[17] (1) $n = 3$: Frequency 9.15307 GHz, Microwave power 1.06 mW, modulation width 1 mT, Amplitude 63–2000 (from 10 K to 150 K) (2) $n = 4$: 9.15811 GHz, 1.00 mW, 0.1 mT, 2–1000 (from 10 K to 160 K) (3) $n = 5$: 9.16210 GHz, 1.00 mW, 0.5 mT, 160–630 (from 14 K to 206 K) (4) $n = 6$: 9.16754 GHz, 1.01 mW, 0.02 mT, 250–1000 (from 10 K to 91 K).
[18] C. P. Slichter, *Principles of Magnetic Resonance*, Springer-Verlag, Berlin, Heidelberg, **2000**.
[19] T. Bichall, K. M. Tnn, *Inorg. Chem.* **1976**, *15*, 376–380.
[20] F. P. Dwyer, A. M. Sargeson, *J. Am. Chem. Soc.* **1959**, *81*, 2335–2336.
[21] Y. Ono, *Doctoral Thesis*, The University of Tokyo, **2004**.
[22] C. Mathonière, C. J. Nuttall, S. G. Carling, P. Day, *Inorg. Chem.* **1996**, *35*, 1201–1206.
[23] Y. Kobayashi, M. Itoi, N. Kojima, K. Asai, *J. Magn. Magn. Mater.* **2004**, *272–276*, 1091–1092.
[24] B. Mayoh, P. Day, *J. Chem. Soc., Dalton Trans.* **1974**, 846–852.
[25] B. Mayoh, P. Day, *J. Chem. Soc., Dalton Trans.* **1976**, 1483–1486.
[26] T. Oguchi, *Statistical Theory of Magnetism*, SYŌKABŌ, 1st ed., **1970**, ch. 4.
[27] H. O. Jones, H. S. Tasker, *J. Chem. Soc., Trans.* **1910**, *95*, 1904–1909.
[28] C. S. Robinson, H. O. Jones, *J. Chem. Soc., Trans.* **1912**, *101*, 62–76.
[29] The number ($n = 3$) of the water of crystallization in $KBa[Fe^{III}(C_2O_2S_2)_3]\cdot nH_2O$ was determined by TG analysis.
[30] D. Coucouvanis, D. Piltingsrud, *J. Am. Chem. Soc.* **1973**, *95*, 5556–5563.
[31] E. Nishibori, M. Takata, K. Kato, M. Sakata, Y. Kubota, S. Aoyagi, Y. Kuroiwa, M. Yamamoto, N. Ikeda, The Large Debye–Scherrer Camera Installed at SPring-8 BL02B2 for Charge Density Studies, *Nuclear Instruments and Method in Physics Research A* **2001**, pp. 467–468, 1045–1048.
[32] O. Kahn, *Molecular Magnetism*, Wiley-VCH, **1993**, ch.1.

Received: June 25, 2005
Published Online: February 2, 2006

